Large-scale statistics for threshold optimization of optically pumped nanowire lasers

Juan Arturo Alanis,[†] Dhruv Saxena,[‡] Sudha Mokkapati,[‡,¶] Nian Jiang,[‡] Kun Peng,[‡] Xiaoyan Tang,[†] Lan Fu,[‡] Hark Hoe Tan,[‡] Chennupati Jagadish,[‡] and Patrick Parkinson[*,†]

†*School of Physics and Astronomy and the Photon Science Institute, The University of Manchester, Manchester, UK*

‡*Department of Electronic Materials Engineering, Research School of Physics and Engineering, The Australian National University, Canberra, Australia*

¶*School of Physics and Astronomy and the Institute for Compound Semiconductors, Cardiff University, Cardiff, UK*

E-mail: patrick.parkinson@manchester.ac.uk

Abstract

Single nanowire lasers based on bottom-up III-V materials have been shown to exhibit room-temperature near-infrared lasing, making them highly promising for use as nanoscale, silicon-integrable and coherent light sources. While lasing behavior is reproducible, small variations in growth conditions across a substrate arising from the use of bottom-up growth techniques can introduce inter-wire disorder, either through geometric or material inhomogeneity. Nanolasers critically depend on both high material quality and tight dimensional tolerances, and as such, lasing threshold is both sensitive *to*, and a sensitive probe *of* such inhomogeneity. We present an all-optical characterization technique coupled to statistical analysis to correlate geometrical, and

material parameters with lasing threshold. For these multiple-quantum-well nanolasers, it is found that low threshold is closely linked to longer lasing wavelength caused by losses in the core, providing a route to optimized future low-threshold devices. A best-in-group room temperature lasing threshold of $\sim 43\,\mu\mathrm{Jcm}^{-2}$ under pulsed excitation was found, and overall device yields in excess of 50% are measured, demonstrating a promising future for the nanolaser architecture.

Keywords

III-V Nanowire lasers, Photoluminescence, Multiple Quantum Well

Over the past two decades, semiconductor nanowires (NWs) have been intensively studied as active components for nanophotonic devices.[1–3] Given their optical wavelength-scale dimensions, ease of incorporation onto a silicon substrate,[4–10] and heterostructure architecture which leverages decades of experience from planar technology, III-V NWs based on arsenide and phosphide materials are highly promising for applications in light emission,[11,12] modulation[13,14] and detection.[11,15] In particular, NW lasers are of interest as a key component for both high-efficiency lighting and future optoelectronic integrated circuitry.[3,8–10,16,17] The development of high-efficiency, nanoscale and silicon-integrated coherent light sources promises to enable super-"Moore's law" developments[18] in computation by realizing low-power speed-of-light chip-to-chip communication.

While a number of design architectures for nanolasers have been being studied,[19–23] NWs with radial quantum-well (QW) structures have attracted attention for the development of tunable and low-power operation NW lasers.[9,24–26] As opposed to simple core (or core-shell) NWs, which rely on the bulk material in the NW core as both the active region and waveguide,[19,23,27–29] gain in a multiple-quantum-well (MQW) NW laser is enhanced by taking advantage of a two-dimensional density of states (DoS) of the quantum well. Through radial design of the lasing cavity, MQW structures also provide the possibility of producing lasing on specific transverse modes.[24,25,30] As in all complex radial heterostructures, balancing the

design requirements of MQW NW lasers has proven to be challenging; the thickness, placement and number of QWs must be carefully chosen to minimize losses and guarantee mode overlap with the MQW active medium[24,31] in addition to conventional cavity requirements such as end-facet reflectivity and NW length.

In this letter, we describe a novel methodology for identifying the critical limitation on NW laser threshold, via a large-scale statistical study of nanolasers. In contrast to focusing on large numbers for scale-up for device applications,[32] by utilizing the small wire-to-wire inhomogeneity inherent to the NW growth technique, we correlate controllable parameters (QW thickness, NW length, inter-well disorder) with functional performance (lasing threshold). This technique provides a method to determine the influence of different controllable parameters, allowing critical parameters to be identified for optimization. Through a study including over one thousand NWs, we also measure a key parameter for the industrial applicability of all single-NW devices; namely, yield. Finally, we are able to identify the best performing nanolaser from within the measurement batch, providing an indication of the upper limit on nanolaser performance within this growth approach.

For the specific case of GaAs/AlGaAs MQW nanolasers designed and grown as described by Saxena et al.,[24] we identify variations in lasing wavelength as the critical limitation to high and uniform yield, along with the influence of quantum well electronic disorder. We measure a minimum room-temperature lasing threshold of $\sim 43\,\mu\mathrm{Jcm}^{-2}$ under pulsed excitation, attributed to a NW with optimal reflectivity, low absorption in the core and high gain-mode overlap. Coupled with an overall yield of over 50% of NWs exhibiting stable lasing behavior under pulsed optical excitation at room-temperature, our results demonstrate a strong future for the single NW laser architecture.

A set of MQW NW lasers with an 80 nm GaAs core, 8 $\mathrm{Al}_x\mathrm{Ga}_{(1-x)}\mathrm{As}$/GaAs quantum wells (with $x = 0.42$ and a nominal thickness of 3.5 ± 1.5 nm) and a 5 nm GaAs capping layer were grown following a published recipe.[24] Full details and transmission electron microscopy have previously been reported.[24] The NWs were transferred onto a z-cut quartz substrate

by gentle rubbing. A representative sample of 31 transferred NWs were measured to have lengths of $3.36 \pm 0.36\,\mu$m and diameters of $464 \pm 14\,$nm using scanning electron microscopy (see **Supporting Information** for details and images). These values are within the original design parameters, but are somewhat shorter than the $5\,\mu$m predicted, possibly due to the mechanical transfer method. For optical measurements, approximately ∼10000 NWs were first identified using optical-microscopy machine-vision and image processing based on an approach modified from optical astronomy.[33] Each NW was imaged, and a low-power photoluminescence spectrum was taken (full experimental details are given in the methods section). A set of 1025 NWs was randomly selected from the ∼10000 full set for in-depth study. For each wire, the low-power photoluminescence spectrum was fit to a simple two-component model following a published approach[31] (see **Supporting Information** for full details), with the first component being core emission and the second being MQW emission. The former comprises the convolution of a 3D density of states (DoS) B_{core} and Gaussian distribution G_{core} for the core emission. For the MQW region the convolution of a 2D density of states B_{MQW} and Gaussian distribution G_{MQW} is used. The final model is taken as the linear combination of both the core and the MQW region multiplied by the correction factors α_{core} and α_{MQW} respectively such that:

$$I(E) = \alpha_{\mathrm{core}}(B_{\mathrm{core}}(E) * G_{\mathrm{core}}(E)) + \alpha_{\mathrm{MQW}}(B_{\mathrm{MQW}}(E) * G_{\mathrm{MQW}}(E)) \quad (1)$$

A typical fit to a PL spectrum is shown in Figure 1a). A number of parameters were determined: E_{core} and $E_{MQW}^{e_1 \rightarrow hh_1}$, the core material band-gap and lowest quantum-well transition energy, σ_{core} and σ_{MQW}, the electronic disorder parameters for the core and quantum-well transition respectively. The electronic temperature T was fixed at room temperature for these low excitation-fluence measurements. The electronic disorder parameters describe a Gaussian convolution on the idealized emission - for the quantum well emission this disorder may arise from fluctuations in well thickness or barrier height (due to Al variation)[34]

in a single well, or due to systematic variations in well thickness between wells in a single wire. For the core, σ_{core} may be attributed to inhomogeneity in strain or stoichiometry along the length of the NW.[35] Taken together, the disorder parameters represent deviation from uniformity, and have been previously shown to be important parameters in describing the emission of quantum-well NWs.[31]

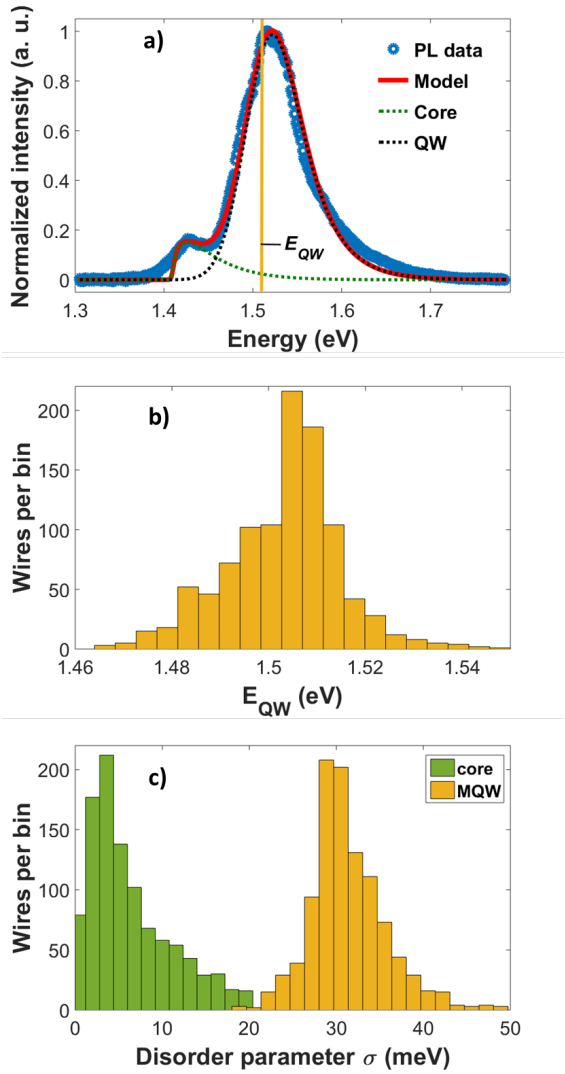

Figure 1: a) Normalized photoluminescence spectrum of a typical NW showing the fitted model (red line); the green and black dotted lines correspond to the core and MQW components respectively. b) Histogram showing the occurrence of the calculated QW energy for the 1025 NWs dataset. The mean emission energy is 1.503 eV. c) Histogram showing the core and QW disorder parameters extracted from the model (provided in the main text) for the same NW set.

The model fit is able to well reproduce the photoluminescence lineshape for the MQW NWs as demonstrated in Figure 1a); it is noted that a deviation at low energy (around 1.4 eV) has been previously observed,[31,36,37] and may be attributable to defects in the GaAs region, while a slight shoulder at higher energy (around 1.6 eV) can be attributed to the higher lying $E_{MQW}^{e_1 \rightarrow lh_1}$ light hole transition. While each NW has 8 quantum wells, each with a potentially different $E_{MQW}^{e_1 \rightarrow hh_1}$, we choose to model the QW photoluminescence as an emitter with a single effective emission energy and disorder; the wires have been designed and previously characterized as having minimal well-to-well thickness variation within a single wire.[24] However, it has been shown that radial growth rates in MOCVD are correlated with the NW core diameter,[38] allowing for wire-to-wire variation in QW emission to occur. As such, to a first order approximation we treat every quantum well in each given NW as identical, but allow these to vary between wires. Any residual intra-wire inhomogeneity in $E_{MQW}^{e_1 \rightarrow hh_1}$ transition energy between wells is expected to appear as an increase in electronic disorder σ_{MQW}.

Figure 1b) shows a histogram of the $E_{MQW}^{e_1 \rightarrow hh_1}$ parameters calculated from 1025 NWs. The obtained values show a range of QW energies varying around a mean of 1.503 eV, indicating a relatively small spread in QW width between wires. Low power PL analysis was performed on a single NW from the same growth by Saxena et al., who reported a QW energy of 1.524 eV (corresponding to a QW width of $\sim$ 5 nm);[24] this measurement lies within the range of energies shown in Figure 1b), but may also be indicative of a slight variation in well thickness because the NWs are sampled from a different area of the growth wafer. A finite-well model was used to calculate the well thickness distribution from the emission energies; a median thickness of $5.6^{+0.93}_{-0.26}$ nm was determined (data shown in the **Supporting Information** ; upper and lower limits describe the interquartile range).

Figure 1c) shows the distribution in core and QW energy disorder. It is notable that the value for QW disorder is similar to that previously reported for a single quantum-well NWs,[31] further confirming a negligible contribution from intrawire well-to-well thickness variation.

The trend for the QW to exhibit an increased disorder over that of the core is in agreement with previous work,[31] where this was attributed to both an increased sensitivity of quantum well confined state energies to thickness disorder and to interface effects.

Lasing behavior was probed using defocussed optical excitation at 620 nm with ∼170 fs pulses at 200 kHz, where the pump pulse diameter was set to be 4-5× larger than the typical NW length to ensure uniform excitation (more details are given in the methods section). It is noted that no special attention was paid to the relative orientation of the NW axis (as determined from optical microscopy) with respect to the excitation polarization. However, no correlation between orientation and threshold was observed, which is likely due to their large diameter and hence small polarization dependence of absorption in these wires.[39] By measuring the power-dependent photoluminescence at room temperature, spectrally resolved light-in light-out (LILO) responses were recorded for the 1025 NWs as shown in Figure 2a). Nanowires were classified as lasing when two conditions were satisfied; a significant increase in gradient is observed on the LILO curve, and the appearance of a narrow emission peak (<6 nm FWHM, limited by the spectral resolution of the spectrometer and with a peak height of over 30% of the overall PL). The pump fluence at threshold was conservatively approximated as the knee of the LILO curve, taking the intersection between a linear fit to the stimulated emission and the spontaneous regimes as shown in the inset of Figure 2a (more details are provided in the **Supporting Information**). For each wire, measurements were halted soon after threshold was reached to avoid laser damage. In total, 579 NWs - 56% of wires - were identified to show lasing at room temperature. Under high excitation fluence, the remaining NWs exhibited a decrease in integrated emission intensity with increasing excitation fluence likely due to carrier overflow from QWs and – ultimately – thermal degradation. For the full statistical analysis, additional filtering was done to remove ∼7% of the 579 NWs where the data was unable to be fitted with sufficient accuracy using our model; this narrowed down the number of NWs used to 534 .

The power-dependent photoluminescence for a low-threshold NW is shown in Figure 2a).

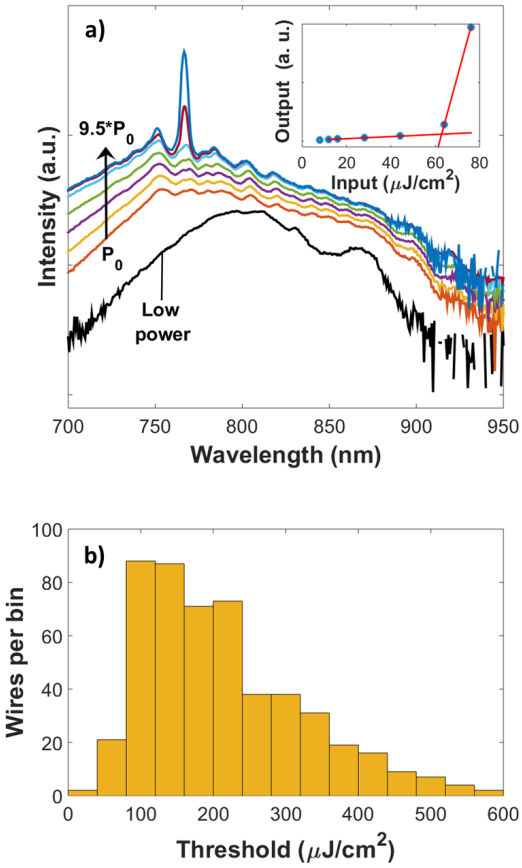

Figure 2: a) Power dependent PL spectra of a selected low-threshold NW laser, where the lowest excitation fluence is indicated as $P_0 = 8\,\mu\mathrm{Jcm}^{-2}$ per pulse. The lowest curve (in black) shows the PL spectrum measured under low-power continuous excitation for the same wire. Inset: LILO curve. An abrupt change in slope is observed at $63\,\mu\mathrm{Jcm}^{-2}$, associated with the transition to lasing behavior. b) A histogram of threshold pump values calculated for 579 lasing NWs.

Single mode lasing was observed at 766.6 nm and pump power at threshold was determined to be 63 μJcm^{-2} per pulse. Below threshold, periodic oscillations in the emission intensity as a function of wavelength is likely due to amplified spontaneous emission of cavity modes. The black line in Figure 2a) corresponds to the low power PL for this particular wire; two peaks, at ∼810nm and ∼870 nm, can be identified as the MQW and core emission respectively. The low power PL emission of the MQW region corresponds to the $e_1 \rightarrow hh_1$ transitions, whereas the lasing wavelength is a combination of the material gain and both longitudinal and transverse cavity modes, related to NW length and diameter, respectively. This can be clearly seen from the main lasing peak at a wavelength of ∼770 nm, significantly blue-shifted from the low power PL emission maxima. Analysis of this data provides a number of new parameters, primarily P_{th}, the lasing threshold and λ_{max}, the lasing wavelength. Figure 2b) illustrates a key result for the future commercial application of III-V nanolasers, in that of the ∼50% of NWs which showed room-temperature lasing, a median P_{th} is found to be $192^{+45}_{-60}\,\mu$Jcm^{-2} where the uncertainty describes the interquartile range. It is striking that the distribution is heavily skewed towards lower threshold. The relationship between excitation pulse energy and material gain is strongly sub-linear,[24] leading to any distribution in threshold gain due to variations in underlying geometry or material quality being amplified when measured in the pulse energy domain. These values are in strong agreement with a previous measurement of $P_{\mathrm{th}} = 110\,\mu$Jcm^{-2} under pulsed 522 nm excitation,[24] with the shorter excitation wavelength used in that work leading to slightly increased optical absorption and thus a reduced threshold.

While, in general, approaches exist to identify the specific geometrical (i.e. reflectivity, waveguide losses) or material (i.e. gain-related) origin for threshold gain and hence P_{th}, techniques such as changing output coupling[40] have no obvious analog for nanolasers. Key parameters such as the reflectivity of end-facets, mode-gain overlap or waveguide losses through substrate coupling can be modeled, but are subject to an unknown level of real-world wire-to-wire disorder in the NW architecture. End-facets are dependent on the precision of

the cleaving process (at the base) and NW growth during the cool-down period (at the tip), while mode-gain overlap may depend upon the diameter of the wire which is a product of the initial seed size inhomogeneity and the NW growth density[38,41–43] or on electronic disorder between quantum wells. While some aspects may be optimized through additional post-growth steps, for instance planarization and polishing for improving end facet reflectivity, it is essential to know which aspects play the most significant role in determining P_{th}.

The threshold gain (g_{th}) required for lasing in a two mirror cavity can be approximated by

$$g_{\mathrm{th}} = \alpha_0 - \frac{\log\left(R_{\mathrm{tip}} R_{\mathrm{base}}\right)}{2L}, \tag{2}$$

where α_0 is the distributed losses, L is the cavity length and R_{tip} and R_{base} are the power reflectivity of the tip and base facets, respectively. The relationship between incident fluence and model gain is, in general, highly non-linear.[24] However, we can seek correlations between threshold incident pulse energy P_{th} and other measurable parameters, as a monotonic relationship is predicted. In the limiting case of a low α_0, constant R values and linear absorption, we would expect an inverse correlation between cavity length and P_{th}. To investigate this, we first determine NW cavity length L_{FP} from laser peak spacing using a Fabry-Perot model:[44]

$$L_{\mathrm{FP}} = \left(\frac{\lambda_0^2}{2\Delta\lambda}\right)\left(n_g - \lambda_0\left(\frac{dn_g}{d\lambda}\right)\right)^{-1}, \tag{3}$$

where λ_0 is the primary laser peak, $\Delta\lambda$ is the longitudinal mode spacing, n_g is the modal refractive index and $dn_g/d\lambda$ is the dispersion (see **Supporting Information** for full details). A value of $n_g = 4.7$ and $dn_g/d\lambda = -0.003$ are used, as determined by numerical modeling.[24] We are limited to 477 NWs for length dependence studies, as two or more longitudinal peaks must be identifiable to use Equation 3. Figure 3a shows a two-dimensional histogram of the lasing threshold and NW length; while a very slight negative correlation is shown (correlation coefficient $\rho = -0.08$, significance value $p = 0.08$), it is not significant at the ($p < 0.01$) level. This weak correlation suggests that distributed losses may dominate,

and/or wire-to-wire disorder in reflectivity is large: If losses which scale with the length of the nanowire dominate (such as waveguide leakage or reabsorption in the core or cap), we would not expect to observe a positive length dependence. SEM images taken from 30 NWs (Supplementary Information) show varied non-planar end faces which may introduce wire-to-wire variation in reflectivity, which in turn may obscure any length dependence.

A much stronger correlation is observed for threshold and lasing wavelength, as shown in Figure 3b. This strong correlation ($\rho = -0.39$, $p < 0.001$) indicates a dramatic increase in threshold for NWs which lase at shorter wavelength; this effect is inherent to the design of our MQW nanolasers. With a GaAs core and GaAs cap, leakage of the TE_{01} mode into the center or edge of the NW leads to a large increase in absorption losses, with losses proportional to the absorption coefficient of GaAs at the lasing wavelength. It is unlikely that waveguiding losses play a large role in this correlation; a narrow observed spread in diameter of 464 ± 7 nm is not expected to lead to a significant variation in cavity confinement, and waveguiding losses for the TE_{01} mode are expected to be small for NW diameters over 400 nm. This behavior is striking, however a note of caution must be struck – increasing the lasing wavelength requires a reduction in electron confinement and associated reduction in gain, and a balance must be sought. It is noted that controlling the lasing wavelength requires both accurate control over the well width, as well as a element of control over the NW length. The Fabry-Perot cavities presented (averaging around 4 μm) impose a minimum longitudinal mode separation of $\sim$12 nm and an associated inhomogeneity in emission wavelength on this scale. A minimization in lasing wavelength disorder would reduce the spread in threshold for a given well disorder, which might be best achieved through the use of longer nanolasers.

A highly important measure for all laser structures is the quality of the gain region; we assess this using the QW disorder parameter σ_{QW} as a proxy, noting that disorder in a quantum well is indicative of any spatial spread in $E_{MQW}^{e_1 \rightarrow hh_1}$ (possibly due to facet-induced growth rate differences[38]) and a corresponding decrease in the density of states for a given emission energy. Figure 3c shows a statistically significant positive correlation between σ_{QW}

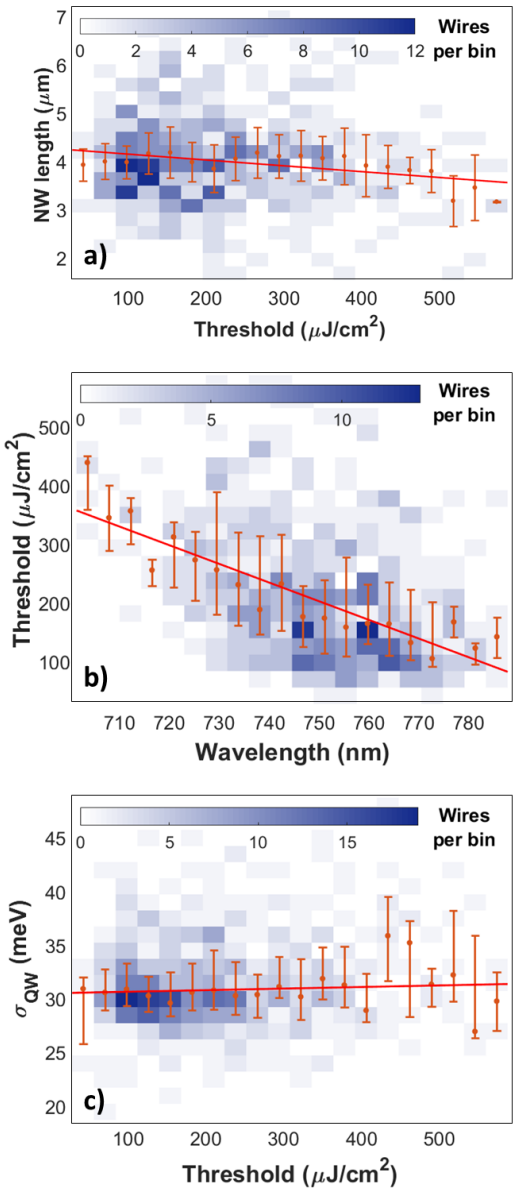

Figure 3: Two-dimensional histogram of a) NW length vs threshold, b) threshold pump power versus lasing wavelength and c) QW disorder parameter versus threshold pump power. The mean value per bin in each panel is shown by the orange points with 1 interquartile range error bars; wires per bin are given by the intensity at each point. A linear guide to the eye is shown as a red line for every case.

and P_{th} ($\rho = 0.14$, $p = 0.002$), leading to a second finding: targeting a reduced QWT disorder is expected to be beneficial for reducing threshold. The effects of inhomogeneity in GaAs/AlGaAs quantum-well systems is well known to increase with decreasing width[45] (see **Supporting Information** Figure S4), however, observed disorders are significantly higher than for comparable planar systems. While we have previously shown that two strategies to limit σ_{QW} are through reducing core disorder to improve intra-wire σ_{QW} or increasing the radial growth rate to reduce inter-wire disorder,[31] we do not see evidence of the former approach for the present NWs (see **Supporting Information** for details). This is likely due to the more effective screening of the effect of core geometrical inhomogeneity on quantum well emission by the significantly thicker barrier layers in the present study. It is notable that variation in threshold as a function of σ_{QW} is small in comparison with the overall dispersion in threshold seen in the nanolaser population.

After controlling the lasing wavelength and quantum well disorder, a residual spread in threshold is most likely due to variations in end-facet reflectivity. It has been noted that in core-shell NW lasers, reflectivity losses are expected to dominate over distributed losses[46,47] due to the small cavity length and typically poor reflectivity, and in those nanolasers, threshold gain is expected to be a strong function of NW length. While the SEM study of 31 NWs (given in the **Supporting Information**) show that end faceting does not subjectively appear to be optimum for lasing, it appears to be of secondary concern to lasing wavelength and QW disorder for the MQW nanolasers described here. It is also noted that for longer wires, tapering remains to be fully controlled which may contribute to an unintended reduction in material gain for wires longer than $4\,\mu$m.

In summary, we have presented an all-optical statistical technique for studying functional optoelectronic nanomaterials. We have applied this methodology to MQW nanolasers based on the GaAs/AlGaAs material system, and have shown both high yield operation of around 50% and optically-pumped room-temperature thresholds of $\sim 43\,\mu\mathrm{Jcm}^{-2}$. As far as we are aware, this is the lowest value reported for this architecture to date. By

correlating geometrical and material parameters across 534 NWs we have identified lasing wavelength and quantum well disorder as key controllable parameters to design for more uniform low-threshold operation. These parameters are rationalized in terms of their impact upon distributed losses and variations in gain, and we make two recommendations for optimization within the presented architecture: to design thicker wells with reduced disorder, and to target longer wires to reduce cavity mode separation. Our methodology can be combined with electron microscopy to assess wire-to-wire variation in threshold resulting from variations in nanowire morphology. The presented large-scale approach is both widely applicable and highly important to obtain yield histograms for any future industrial applicability. It is observed that MQW wires grown via Au-assisted vapor-liquid-solid metal-organic vapor-phase-epitaxy show both a reasonably high yield and threshold disorder, supporting their potential future implementation into optoelectronic integrated circuitry.

Methods

Micro-photoluminescence: Automated micro-photoluminescence measurements were carried out using a home built microscope system as described in detail in the **Supporting Information** . The system is equipped with two laser sources; a HeNe laser (632.8 nm) for low-power photoluminescence measurements, and a pulsed 620 nm 170 fs 200 kHz laser derived from a Coherent RegA and optical parametric amplifier. The pulsed laser beam was defocussed to produce a spot of around 20 μm diameter to ensure complete excitation of the NWs. The spectral response of the system was corrected using a tungsten bulb.

Scanning Electron Microscopy: Scanning electron microscopy images were taken using an FEI Helios 600 at the Australian National Fabrication Facility (ACT Node). Images were taken on the same sample as the optical measurements, where a $\sim$2-5 nm thick mixed metal Pt/Au layer was first deposited to avoid sample charging.

Data analysis: The data was analysed as described in the text and **Supporting Information** , using 2D correlation analysis provided by the MATLAB package. All reported correlation (ρ) values are determined from Pearson linear correlation analysis, and values are determined to be significant when ($p < 0.01$).

Author Contributions

The project was conceived by PP, and the data was primarily taken and analyzed by JAA. XT contributed additional analysis. The nanolasers were designed by DS and SM, and grown by NJ under the supervision of HHT and CJ. Scanning electron microscopy was performed by KP under the supervision of LF. The manuscript was primarily written by JAA and PP, with contributions from all authors.

Acknowledgement

We thank the Australian National Fabrication Facility (ANFF) ACT node for access to the epitaxy, fabrication and characterization facilities used in this work. PP acknowledges the support of the Royal Society (RG140411). JAA acknowledges a CONACyT-funded scholarship. PP acknowledges Joe Zuntz and Philip Dawson (University of Manchester) for useful discussions.

Supporting Information Available

Detailed experimental arrangement, Photoluminescence model, Fabry-Perot length calculations, Scanning Electron Microscopy imaging and details, Quantum Well thickness calculations and Additional correlations. This material is available free of charge via the Internet at `http://pubs.acs.org/`.

References

(1) Joyce, H. J.; Gao, Q.; Hoe Tan, H.; Jagadish, C.; Kim, Y.; Zou, J.; Smith, L. M.; Jackson, H. E.; Yarrison-Rice, J. M.; Parkinson, P.; Johnston, M. B. *Progress in Quantum Electronics* **2011**, *35*, 23–75.

(2) Dasgupta, N. P.; Sun, J.; Liu, C.; Brittman, S.; Andrews, S. C.; Lim, J.; Gao, H.; Yan, R.; Yang, P. *Advanced materials (Deerfield Beach, Fla.)* **2014**, *26*, 2137–84.

(3) Yang, P.; Yan, R.; Fardy, M. *Nano letters* **2010**, *10*, 1529–36.

(4) Tomioka, K.; Kobayashi, Y.; Motohisa, J.; Hara, S.; Fukui, T. *Nanotechnology* **2009**, *20*, 145302.

(5) Koblmüller, G.; Abstreiter, G. *physica status solidi (RRL) - Rapid Research Letters* **2014**, *8*, 11–30.

(6) Kim, S.-K.; Zhang, X.; Hill, D.; Song, K.-D.; Park, J.-S.; Park, H.-G.; Cahoon, J. F. *Nano letters* **2015**, *15*, 753.

(7) Mayer, B.; Janker, L.; Loitsch, B.; Treu, J.; Kostenbader, T.; Lichtmannecker, S.; Reichert, T.; Morkötter, S.; Kaniber, M.; Abstreiter, G.; Gies, C.; Koblmüller, G.; Finley, J. J. *Nano Letters* **2016**, *16*, 152–156.

(8) Kim, H.; Lee, W.-J.; Farrell, A. C.; Morales, J. S. D.; Senanayake, P.; Prikhodko, S. V.; Ochalski, T. J.; Huffaker, D. L. *Nano Letters* **2017**, acs.nanolett.7b00384.

(9) Lu, F.; Bhattacharya, I.; Sun, H.; Tran, T.-T. D.; Ng, K. W.; Malheiros-Silveira, G. N.; Chang-Hasnain, C. *Optica* **2017**, *4*, 717.

(10) Chen, B.; Wu, H.; Xin, C.; Dai, D.; Tong, L. *Nature Communications* **2017**, *8*, 20.

(11) Chuang, L. C.; Sedgwick, F. G.; Chen, R.; Ko, W. S.; Moewe, M.; Ng, K. W.; Tran, T.-T. D.; Chang-Hasnain, C. *Nano Letters* **2011**, *11*, 385–390.

(12) Yuan, X.; Saxena, D.; Caroff, P.; Wang, F.; Lockrey, M.; Mokkapati, S.; Tan, H. H.; Jagadish, C. *The Journal of Physical Chemistry C* **2017**, acs.jpcc.7b00744.

(13) Greytak, A. B.; Barrelet, C. J.; Li, Y.; Lieber, C. M. *Applied Physics Letters* **2005**, *87*, 151103.

(14) Baig, S. A.; Boland, J. L.; Damry, D. A.; Tan, H. H.; Jagadish, C.; Joyce, H. J.; Johnston, M. B. *Nano Letters* **2017**, acs.nanolett.7b00401.

(15) Wang, J. *Science* **2001**, *293*, 1455–1457.

(16) Tchernycheva, M.; Messanvi, A.; De Luna Bugallo, A.; Jacopin, G.; Lavenus, P.; Rigutti, L.; Zhang, H.; Halioua, Y.; Julien, F. H.; Eymery, J.; Durand, C. *Nano Letters* **2014**, *14*, 3515–3520.

(17) Berm??dez-Ure??a, E.; Tutuncuoglu, G.; Cuerda, J.; Smith, C. L. C.; Bravo-Abad, J.; Bozhevolnyi, S. I.; FontcubertaMorral, A.; Garc??a-Vidal, F. J.; Quidant, R. *Nano Letters* **2017**, *17*, 747–754.

(18) Sun, C. et al. *Nature* **2015**, *528*, 534–538.

(19) Saxena, D.; Mokkapati, S.; Parkinson, P.; Jiang, N.; Gao, Q.; Tan, H. H.; Jagadish, C. *Nature Photonics* **2013**, *7*, 963–968.

(20) Huang, M. H.; Mao, S.; Feick, H.; Yan, H.; Wu, Y.; Kind, H.; Weber, E.; Russo, R.; Yang, P. *Science (New York, N.Y.)* **2001**, *292*, 1897–9.

(21) Burgess, T.; Saxena, D.; Mokkapati, S.; Li, Z.; Hall, C. R.; Davis, J. A.; Wang, Y.; Smith, L. M.; Fu, L.; Caroff, P.; Tan, H. H.; Jagadish, C. *Nature Communications* **2016**, *7*, 11927.

(22) Mayer, B.; Janker, L.; Rudolph, D.; Loitsch, B.; Kostenbader, T.; Abstreiter, G.; Koblmüller, G.; Finley, J. J. *Applied Physics Letters* **2016**, *108*, 071107.

(23) Sergent, S.; Takiguchi, M.; Tsuchizawa, T.; Taniyama, H.; Kuramochi, E.; Notomi, M. **2017**,

(24) Saxena, D.; Jiang, N.; Yuan, X.; Mokkapati, S.; Guo, Y.; Tan, H. H.; Jagadish, C. *Nano Letters* **2016**, *16*, 5080–5086.

(25) Stettner, T.; Zimmermann, P.; Loitsch, B.; Döblinger, M.; Regler, A.; Mayer, B.; Winnerl, J.; Matich, S.; Riedl, H.; Kaniber, M.; Abstreiter, G.; Koblmüller, G.; Finley, J. J. *Applied Physics Letters* **2016**, *108*, 011108.

(26) Schuster, F.; Kapraun, J.; Malheiros-Silveira, G. N.; Deshpande, S.; Chang-Hasnain, C. J. *Nano Letters* **2017**, acs.nanolett.7b00607.

(27) Ho, J.; Tatebayashi, J.; Sergent, S.; Fong, C. F.; Iwamoto, S.; Arakawa, Y. *ACS Photonics* **2015**, *2*, 165–171.

(28) Mandl, M.; Wang, X.; Schimpke, T.; Kölper, C.; Binder, M.; Ledig, J.; Waag, A.; Kong, X.; Trampert, A.; Bertram, F.; Christen, J.; Barbagini, F.; Calleja, E.; Strassburg, M. *physica status solidi (RRL) - Rapid Research Letters* **2013**, *7*, 800–814.

(29) Chen, S.; Jansson, M.; Stehr, J. E.; Huang, Y.; Ishikawa, F.; Chen, W. M.; Buyanova, I. A. *Nano Letters* **2017**, *17*, 1775–1781.

(30) Qian, F.; Li, Y.; Gradečak, S.; Park, H.-G.; Dong, Y.; Ding, Y.; Wang, Z. L.; Lieber, C. M. *Nature Materials* **2008**, *7*, 701–706.

(31) Davies, C. L.; Parkinson, P.; Jiang, N.; Boland, J. L.; Conesa-Boj, S.; Tan, H. H.; Jagadish, C.; Herz, L. M.; Johnston, M. B. *Nanoscale* **2015**, *7*, 20531–20538.

(32) Blanc, P.; Heiss, M.; Colombo, C.; Mallorquì, A. D.; Safaei, T. S.; Krogstrup, P.; Nygard, J.; Morral, A. F. i. *International Journal of Nanotechnology* **2013**, *10*, 419.

(33) Bertin, E.; Arnouts, S. *Astronomy and Astrophysics Supplement Series* **1996**, *117*, 393–404.

(34) Shi, T.; Jackson, H. E.; Smith, L. M.; Jiang, N.; Gao, Q.; Tan, H. H.; Jagadish, C.; Zheng, C.; Etheridge, J. *Nano Letters* **2015**, *15*, 1876–1882.

(35) Joyce, H. J.; Gao, Q.; Tan, H. H.; Jagadish, C.; Kim, Y.; Zhang, X.; Guo, Y.; Zou, J. *Nano Letters* **2007**, *7*, 921–926.

(36) Chen, Y.; Cingolani, R.; Andreani, L. C.; Bassani, F.; Massies, J. *Il Nuovo Cimento D* **1988**, *10*, 847–859.

(37) Bolinsson, J.; Ek, M.; Trägårdh, J.; Mergenthaler, K.; Jacobsson, D.; Pistol, M. E.; Samuelson, L.; Gustafsson, A. *Nano Research* **2014**, *7*, 1–18.

(38) Zheng, C.; Wong-Leung, J.; Gao, Q.; Tan, H. H.; Jagadish, C.; Etheridge, J. *Nano Letters* **2013**, *13*, 3742–3748.

(39) Chen, G.; Wu, J.; Lu, Q.; Gutierrez, H. R.; Xiong, Q.; Pellen, M. E.; Petko, J. S.; Werner, D. H.; Eklund, P. C. *Nano Letters* **2008**, *8*, 1341–1346.

(40) Findlay, D.; Clay, R. *Physics Letters* **1966**, *20*, 277–278.

(41) Jensen, L. E.; Björk, M. T.; Jeppesen, S.; Persson, A. I.; Ohlsson, B. J.; Samuelson, L. *Nano Letters* **2004**, *4*, 1961–1964.

(42) Noborisaka, J.; Motohisa, J.; Fukui, T. *Applied Physics Letters* **2005**, *86*, 213102.

(43) Zhang, Y.; Aagesen, M.; Holm, J. V.; J??rgensen, H. I.; Wu, J.; Liu, H. *Nano Letters* **2013**, *13*, 3897–3902.

(44) Dobrovolsky, A.; Stehr, J. E.; Sukrittanon, S.; Kuang, Y.; Tu, C. W.; Chen, W. M.; Buyanova, I. A. *Small* **2015**, *11*, 6331–6337.

(45) Weisbuch, C.; Dingle, R.; Gossard, A.; Wiegmann, W. *Solid State Communications* **1981**, *38*, 709–712.

(46) Zimmler, M. a.; Capasso, F.; Müller, S.; Ronning, C. *Semiconductor Science and Technology* **2010**, *25*, 024001.

(47) Maslov, A. V.; Ning, C. Z. *Applied Physics Letters* **2003**, *83*, 1237–1239.

Graphical TOC Entry